

PACS numbers: 42.55.Px; 42.60.Da; 41.75.Fr
DOI: 10.1070/QE2009v039n11ABEH014159

Simulation of a longitudinally electron-beam-pumped nanoheterostructure semiconductor laser

D.V. Vysotsky, N.N. Elkin, A.P. Napartovich, V.I. Kozlovsky, B.M. Lavrushin

Abstract. **A three-dimensional numerical model of a vertical-cavity surface-emitting laser (VCSEL) containing a resonance grating of quantum wells (QWs) is developed. The Helmholtz equation for a field and the diffusion equation for a medium, in which an electron beam is the source of charge carriers, are solved self-consistently, which allowed us to find the longitudinal and radial profiles of the generated field, its frequency, and the threshold pump current. The characteristics of the higher-order modes are calculated against the background of the frozen medium formed by the generated mode. The stability limit of the single-mode regime and the type of a mode at which lasing begins to develop with increasing pump power are found from calculations of the gain balance and losses for higher-order modes. An iteration algorithm is developed for calculating the parameters of a VCSEL with many QWs, the calculation time increasing linearly with the number of QWs. The profiles of the resonator modes and their frequency spectrum are calculated for a cylindrically symmetric VCSEL. The stability limits of single-mode lasing are determined. The results are compared qualitatively with experiments.**

Keywords: *resonance heterostructure, method of counterpropagating beams, eigenvalues, nonlinear operator.*

1. Introduction

Heterostructures containing many quantum wells (QWs) are of practical interest for application in vertical-cavity surface-emitting lasers (VCSELs). They can be pumped either by an electron beam or laser diodes [1]. Longitudinally electron-beam-pumped semiconductor lasers can be used as quasi-continuous monochromatic radiation sources in display tech-nologies. A distinctive feature of such lasers is the absence of optical confinement in the direction perpendicular to the resonator axis. The laser field distribution in the transverse direction is determined by a change in the complex per-mittivity, which in turn is controlled by the current density distribution in an electron beam spot, the scattering of electrons in a semiconductor and the diffusion of charge carriers.

The first theoretical studies of the mode composition and radiation directivity taking into account the spatial transverse inhomogeneity of excitation were performed for a transversely pumped semiconductor laser [2, 3]. Analytic solutions were constructed for the field in the resonator for some characteristic pump rate distributions and the parameters of configuration losses was introduced. These solutions described qualitatively the radiation pattern for the basic types of oscillations upon pumping slightly exceeding the lasing threshold. This approach applied to longitudinally pumped lasers showed [4] that the characteristic transverse size of the field intensity distribution for the fundamental mode at the lasing threshold is smaller than the diameter of an electron beam with the Gaussian current density function.

The laser radiation divergence in experiments noticeably exceeded the diffraction limit, especially when the lasing threshold was considerably exceeded. It was assumed that this was caused by excitation of higher-order modes. The authors of paper [5] calculated the field intensity profiles for transverse modes in the WKB approximation, found their excitation thresholds, and analysed the inhomogeneities of the gain distribution and the role of a thermal lens. The divergence angle of a laser beam for the given current was equated to the divergence angle of the highest excited type of oscillations. The theory explained qualitatively the increase in the divergence angle from $\sim 5^\circ$ at the lasing threshold up to $\sim 15^\circ$ in the case of a considerable excess over the threshold in laser electron-beam tubes with a single-crystal active region and the electron-beam spot diameter 35 μm. However, these papers neglected the influence of the generated field on the distribution of the complex permittivity, which is considerable in semiconductor lasers [6].

In the last years the attention of researchers has shifted from single-crystal structures to nanoheterostructures in which the lasing threshold at room temperature can be considerably reduced by using resonantly periodic amplification [7]. The simulation of a QW grating VCSEL is a challenging computing problem because of a great number of layers with boundaries partially reflecting light and due to the nonlinear type of eigenvalue equations. In addition, a mathematical model of the laser should adequately take into account diffraction intracavity phenomena and match the solutions for the electromagnetic field in QWs with the solutions of nonlinear equations of the diffusion type for current carriers.

D.V. Vysotskii, N.N. Elkin, A.P. Napartovich State Research Center of the Russian Federation, Troitsk Institute for Innovation and Fusion Research, ul. Pushkovykh 12, 142190 Troitsk, Moscow region, Russia; e-mail: dima@triniti.ru;
V.I. Kozlovsky, B.M. Lavrushin P.N. Lebedev Physics Institute, Russian Academy of Sciences, Leninsky prosp. 53, 119991 Moscow, Russia

Received 19 May 2009; revision received 8 July 2009
Kvantovaya Elektronika **39** (11) 1028 – 1032 (2009)
Translated by M.N. Sapozhnikov

In this paper, we describe briefly the iteration algorithm for calculating the parameters of VCSELs with many QWs and calculate the profiles of resonator modes and their frequency spectrum for cylindrical VCSELs. The stability limits for single-mode lasing are determined and qualitative comparison with experiments is performed.

2. Mathematical model of a VCSEL

The general calculation of a VCSEL by the method of count-erpropagating waves [8] considers the propagation of plane waves through a set of homogeneous layers by using the transfer matrix (T-matrix) formalism. The amplitudes of counterpropagating waves on the lower and upper boundaries of the layer set are transformed to each other via the product of the corresponding 2×2 T-matrices. Spatially inhomogeneous fields are expanded in plane waves, and then the T-matrix method is applied to the expansion components. By starting from a certain plane and performing with the help of this transformation a round trip in the cavity, a closed system of equations can be obtained for an unknown function representing the field distribution for a wave of one direction in the selected plane. By using a discrete approximation, the authors of [8] have obtained a matrix equation $Au = 0$ for a finite-dimensional vector u and derived explicit expressions for the elements of the matrix A, which depend on the unknown eigenvalue λ containing the exact value of a cavity mode frequency. The solution of the matrix equation $Au = 0$ is found by the selection of λ. However, this method requires a great memory capacity for explicit calculations of the completely filled matrix A and cannot be applied to the nonlinear regime, which is of most interest in the case of lasers.

The method, which is close ideologically to that described above but is devoid of the disadvantages of the latter, is proposed in paper [9]. The field transformation on passing from one transverse plane to another in a layered medium is described by operators taking into account reflections from intermediate boundaries. The field transformation during propagation through a QW is described by a nonlinear operator, which requires the use of the iteration approach generalising the Fox–Li method [10]. If a heterostructure consists of many QWs, the problem complicates. In this case, it was proposed [11] to use a special iteration procedure leading to a linear dependence of the calculation time on the number of QWs.

Figure 1 shows a heterostructure consisting of a QW grating located between external and lower Bragg mirrors (BMs). Between BMs and the QW grating, thin matching layers are inserted. If the z axis is directed perpendicular to the substrate, then the VCSEL will represent a set of L plane layers $\{[z_{k-1}, z_k], k = 1, ..., L\}$ with boundary coordinates $\{z_k, k = 0, ..., L\}$ and the thickness $h_k = z_k - z_{k-1}$ of the kth layer. The aluminium substrate is numbered in the numerical scheme as a layer with $k = 0$, while the output mirror layer has the number $k = L + 1$. The refractive index and absorption coefficient of all passive layers are assumed homogeneous. Their profiles in QWs are determined by the action of pump and laser radiations.

We assume that polarisation effects can be neglected and restrict ourselves to the scalar diffraction model. In addition, the refraction index and absorption coefficient in the transverse plane are assumed axially symmetric, which makes the use of cylindrical coordinates convenient. The generated

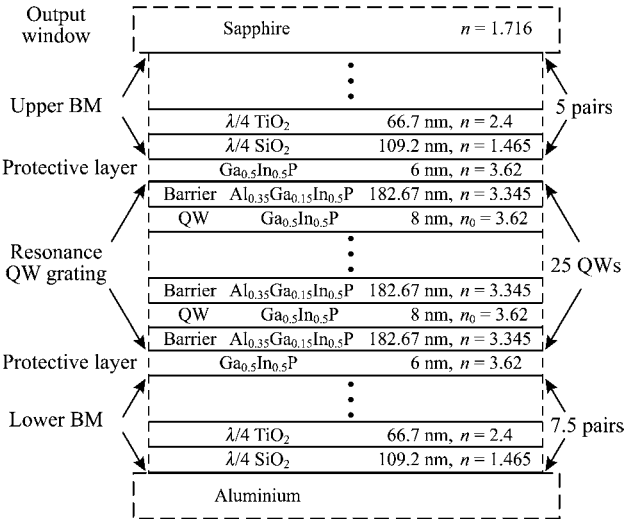

Figure 1. Scheme of a VCSEL. The relative size of layers is shown out of scale.

field depends on time as $E(r, \varphi, z, t) = U(r, \varphi, z) \exp(-i\Omega t)$, where $\Omega = \omega_0 + \Delta\omega - i\delta$; ω_0 is the reference laser frequency; $\Delta\omega = \omega - \omega_0$ is the mode frequency shift; and δ is the decay decrement. The reference frequency ω_0 is selected close to the laser frequency, and the corresponding wave vector and wavelength in vacuum are $k_0 = \omega_0/c$ and $\lambda_0 = 2\pi/k_0$, respectively.

The optical modes of the VCSEL in the adopted approximations are standard TEM_{nm} modes, where m is the angular index corresponding to the dependence $\sim \exp(im\varphi)$ and n is the radial number. By making the substitution $U(r, \varphi, z) = U_m(r, z) \exp(im\varphi)$, we exclude the angular coordinate and obtain the equation

$$\frac{\partial^2 U_m}{\partial z^2} + \frac{1}{r}\frac{\partial}{\partial r}\left(r\frac{\partial U_m}{\partial r}\right) - \frac{m^2}{r^2}U_m + (k_0^2 n^2 - ik_0 g)U_m - ik_0 n^2 \beta U_m = 0, \quad (1)$$

containing the complex eigenvalue β. Here, n and g are the refractive index and gain, respectively; $\beta = g_t + i2\Delta k$; $\Delta k = \Delta\omega/c$; and g_t is the threshold gain.

In the absence of pumping, equation (1) together with conditions at the side boundary $r = r_{max}$ selected far enough from the pump spot determines the optical modes of the passive structure. When the pump energy exceeds the threshold, the self-consistent solution of the wave equation and equations for the medium gives the profile of the generated field and its frequency in the stationary lasing regime. The fundamental mode has the axial symmetry in the case of axially symmetric pumping. Therefore, equation (1) should be solved for $m = 0$ together with the system of nonlinear equations for the diffusion of carries in QWs [12]

$$\frac{1}{r}\frac{\partial}{\partial r}\left(r\frac{\partial Y_j}{\partial r}\right) - \frac{Y_j}{D\tau_{nr}} - \frac{B}{D}N_{tr}Y_j^2 - \frac{|U_0|^2 \ln[\chi(Y_j)]}{D\tau_{nr}} = -\frac{J}{eDdN_{tr}} \quad (2)$$

for the normalised density of carriers $Y_j = N_j/N_{tr}$ in the jth QW, $j = 1, ..., q$. Here, N_j is the carrier density; $N_{tr} =$

$\{-1/\tau_{nr} + [1/\tau_{nr}^2 + 4BJ_{tr}/(ed)]^{1/2}\}/(2B)$ is the carrier density in the case of transparency; D is the diffusion coefficient; τ_{nr} is the recombination time; B is the nonlinearity coefficient; d is the QW thickness; e is the elementary electric charge; $|U_0|^2 = I/I_s$ is the radiation intensity normalised to the saturation intensity $I_s = hcN_{tr}/(\lambda_0 g_0 \tau_{nr})$; $J = \kappa J_{tr} f(r/r_0)$ is the equivalent injection current density producing the same charge carrier flow in the QW as the specified electron beam; J_{tr} is the transparency current density; κ is the pump amplitude; $f(\rho)$ is the pump profile; $f(0) = 1$, $\rho = r/r_0$; r_0 is the pump region radius. The output power of the VCSEL is calculated from the expression $P_{out} = 2\pi \int I_{out} r\,dr$, where I_{out} is the intensity profile of the emitted field. The boundary conditions for $Y_j(r)$ at the side boundaries of active layers ($r = r_{max}$) are set equal to zero. The gain and refractive index in active layers are calculated from approximate expressions

$$g_j = g_0 \ln[\chi(Y_j)],\ n_j = n_0 - \frac{R(g_0 + g_j)}{2k_0},$$
$$\chi(Y) = \begin{cases} \alpha + (1-\alpha)Y^{1/(1-\alpha)}, & Y < 1, \\ Y, & Y \geqslant 1, \end{cases} \tag{3}$$

where g_0 is the gain parameter; n_0 is the refractive index in the absence of charge carriers; R is the line broadening factor; and $\alpha = e^{-1}$.

The densities of the equivalent injection current and electron-beam current are related by the expression

$$\frac{J}{ed} = \frac{\eta j_b E_e}{3E_g N_{qw} ed},$$

where j_b is the axial electron-beam current density; E_e is the energy of electrons in a beam; E_g is the energy gap width of barrier layers; N_{qw} is the number of QWs; $\eta = 0.75$ is the fraction of the pump electron-beam energy supplied to the QW structure. The rest of the energy is carried away by reflected electrons and secondary emission electrons, and also is absorbed in BMs. For experimental parameters $E_e = = 40$ keV, $3E_g = 7.08$ eV, and $N_{qw} = 25$, the densities of the equivalent injection current and electron-beam current are related by the expression

$$J = 170\ \mu A\ cm^{-2} \leftrightarrow j_b = 1\ \mu A\ cm^{-2}.$$

The solution of equation (1) for $m = 0$ together with the corresponding boundary conditions is reduced to the solution of the eigenvalue problem for a nonlinear operator. The additional condition $\delta = 0$ ($\mathrm{Re}\,\beta = 0$) determines the stationary lasing regime. We consider here briefly the numerical method, which is described in more detail in [9]. The wave field in each horizontal plane is represented as the sum of two fields propagating upward and downward over the structure. A quantum well is simulated by a homogeneous layer containing an inhomogeneous phase screen with the gain and phase incursion obtained from equations (2) and (3). Thus, the VCSEL is represented as a set of alternating homo-geneous layers, which are separated in some places by in-homogeneous phase screens. The propagation of the field between two adjacent phase screens is calculated with the help of the Hankel fast transformation algorithm [13] and the T-matrix formalism for Fourier components. Because the beginning of the round trip is selected arbitrarily, a wave propagating upward from the upper QW plane was chosen as the start wave. The condition of the field reproduction after the round trip transit is expressed by the operator equation

$$\boldsymbol{P}(g, n, \beta)u = u \tag{4}$$

for the function u and the eigenvalue β. To find the solution of (4), first the solution of the auxiliary eigenvalue problem

$$\boldsymbol{P}(g, n, \beta)u = \gamma u \tag{5}$$

should be found for the unknown function u and eigenvalue γ for the specified complex value of β. Then, the value of β is selected to obtain the equality $\gamma = 1$ with the specified accuracy. In the absence of pumping, the problem is linear. Because of practical interest are only the highest-Q modes (u, γ), the auxiliary problem can be efficiently solved by the Arnoldy method [14], which does not require the explicit calculation of the $\boldsymbol{P}(g, n, \beta)$ matrix, but requires only the knowledge of the algorithm of action of the operator $\boldsymbol{P}(g, n, \beta)$ on the vector u. The eigenvalue of the nonlinear operator in equation (5) in the lasing regime is modulo 1. The operator $\boldsymbol{P}(g, n, \beta)$ of a round-trip transit in the resonator depends on the distributions of the gain g and refractive index n in QWs, which can be found from equations (2) and (3). This problem is solved by the Fox–Li iteration method [10].

3. Results of calculations and discussion

The reference wavelength used in calculations was $\lambda_0 = = 640$ nm. According to the experiment, the lower BM consisted of 7.5 pairs and the upper mirror consisted of 5 pairs of alternating quarter-wave SiO_2 ($n = 1.465$, $h = 109.2$ nm) and TiO_2 ($n = 2.4$, $h = 66.7$ nm) layers. The active part of the VCSEL contained 25 QWs ($Ga_{0.5}In_{0.5}P$, $n = n_0 = 3.62$, $h = d = 8$ nm) separated by barrier layers ($Al_{0.35}Ga_{0.15}In_{0.5}P$, $n = 3.345$, $h = 182.67$ nm). Thus, the QW grating formed a finite periodic structure with the optical period exactly equal to λ_0, and, therefore, the structure was resonant. Additional 6-nm-thick protective layers with $n = 3.62$ were inserted between the heterostructure and BMs. Finally, the VCSEL was mounted on an aluminium plate and was covered from above by an input sapphire window ($n = 1.716$). Aluminium and sapphire plates in the numerical model were assumed infinite. The rest of the parameters were $D = 0.5\ cm^2\ s^{-1}$, $\tau_{nr} = 10^{-9}$ s, $B = 3.5\times10^{-10}\ cm^3\ s^{-1}$, $r_0 = 13\ \mu m$, $g_0 = 3400\ cm^{-1}$, $J_{tr} = = 400\ A\ cm^{-2}$, which corresponds to the axial density of the transparency current of the electron beam $j_{tr}^b = 2.35\ A\ cm^{-2}$ and the saturation intensity $I_s = 172\ kW\ cm^{-2}$. Because the pump profile in the electron-beam-pumped VCSEL and the line broadening factor are not known accurately, calculations were performed for model profiles $f(\rho) = (1 + \rho^4)^{-1}$ and $f(\rho) = \exp(-\rho^6)$, which did not change over the structure length.

The number of nodes of the radial grid in all calculations presented below was $N_r = 1024$. To estimate the digitization error, one of the variants ($I_b = 35\ \mu A$, $f(\rho) = = (1 + \rho^4)^{-1}$, $R = 2.5$) was recalculated by using a grid with $N_r = 2048$. The relative change in Δk for the TEM_{00} mode was 0.8×10^{-5}, while the relative change in the output power was 3.2×10^{-3}. In the case of a linear problem (reson-ator with a 'frozen' active medium), calculations for the TEM_{01} mode gave the relative change in β at the level 3.4×10^{-5}. Thus, the calculation error is quite acceptable.

We performed a series of calculations for $R = 2.5$. Let us illustrate the results of calculations for the electron-beam current equal to 35 μA and the profile described by the expression $f(\rho) = (1 + \rho^4)^{-1}$. The calculated frequency shift was found to be $\Delta k = -405.36$ см$^{-1}$, which corresponds to the laser wavelength shift with respect to the reference wavelength $\lambda - \lambda_0 = 1.98$ nm. To determine the main reason for the laser wavelength shift, we calculated the eigenfrequencies of the system in the approximation of plane waves of an unlimited aperture. Figure 2 presents the dependence of the resonance wavelength shift on the number of QWs in the structure. In the case of a small number of QWs, the wavelength shift rapidly decreases, which is explained by a decrease in the influence of the boundaries of the QW system, and then saturates. For 25 QWs, the resonance wavelength shift is 2.03 nm and is virtually independent of the electron-beam current.

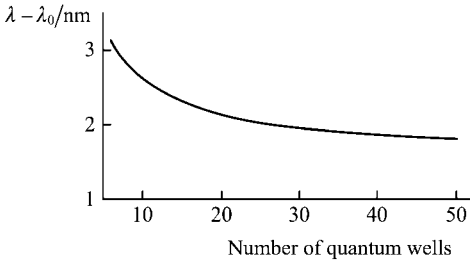

Figure 2. Shift of the resonance wavelength of the VCSEL as a function of the number of QWs in the absence of the transverse structure of the pump and field.

The longitudinal field intensity distribution on the VCSEL axis is shown in Fig. 3. Because the wavelength is close to the resonance wavelength, the heights of field intensity peaks in different QWs are almost the same. Correspondingly, the radial gain profiles are also close in different QWs. The gain profile in the diametrical section of the upper QW is shown in Fig. 4a. The diameter of the region with the positive gain is ~ 30 μm. The dip in the gain profile at the axis is caused by the gain saturation by laser radiation. For comparison, the intensity distribution in the diametrical section of the laser beam is presented in Fig. 4b together with the profile $f(\rho)$. The laser beam diameter at half-maximum is 3.7 μm.

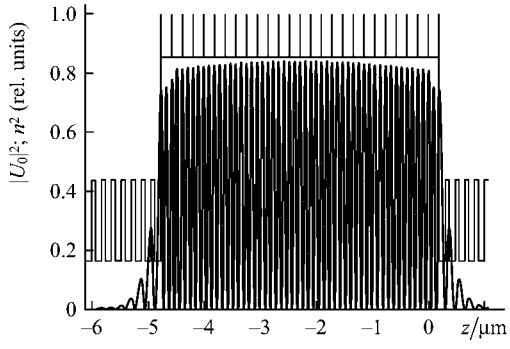

Figure 3. Longitudinal distribution of the field intensity on the axis $r = 0$ (continuous function) and the square of the refractive index (step function); $I_b = 35$ μA, $f(\rho) = (1 + \rho^4)^{-1}$, $R = 2.5$.

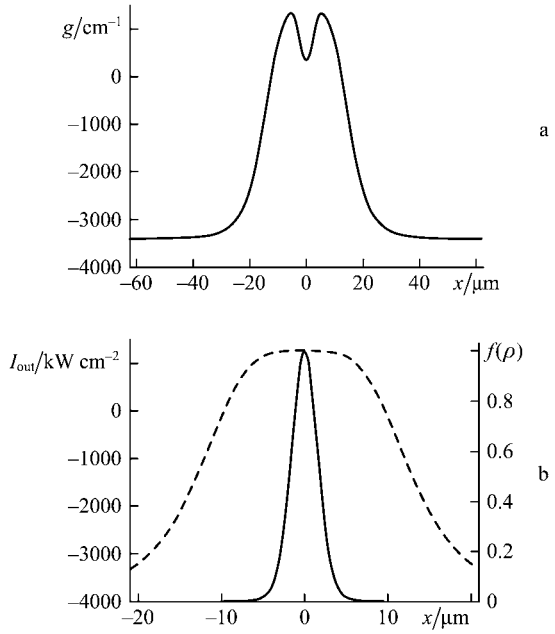

Figure 4. Transverse section of the gain profile in the upper QW (a) and the pump distribution $f(\rho) = (1 + \rho^4)^{-1}$ (solid curve) and the TEM_{00} mode intensity (b); $I_b = 35$ μA, $R = 2.5$.

To estimate effects caused by variations in current, we performed a series of calculations and plotted the watt–ampere characteristic (Fig. 5). By extrapolating the calculated dependence of the laser power to zero, we found the lasing threshold $I_t \approx 32$ μA, which is consistent with the experimental value. The laser beam quality is characterised by the M^2 factor. The calculated dependence of this factor on the pump current (Fig. 5) demonstrates the improvement of the beam quality with increasing current.

The limiting current for stable single-mode lasing can be found by solving a linear eigenvalue problem under condition that the gain and refractive index of the active medium are formed by the laser mode and are 'frozen'. If the threshold gain for some mode (different from the generated mode), including the difference of the gain and total losses, becomes positive, the single-mode lasing stability is violated. Our calculations show that the lasing threshold for the TEM_{01} mode is achieved for $I_b \approx 38$ μA. Thus, single-mode lasing remains stable for currents $I_b \lesssim 1.2 I_t$. At higher currents, the quality of the output radiation decreases due to the development of lasing at higher modes.

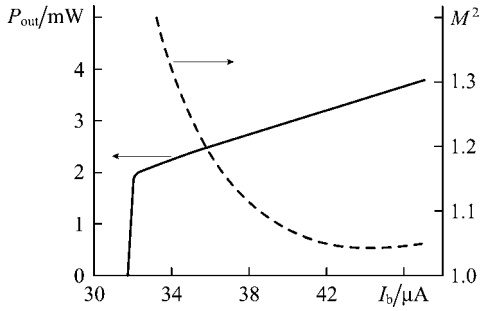

Figure 5. Output power and the M^2-factor of the TEM_{00} mode as functions of the pump current; $f(\rho) = (1 + \rho^4)^{-1}$, $R = 2.5$.

For the hyper-Gaussian pump profile $f(\rho) = \exp(-\rho^6)$, both the threshold pump current (17 μA) and the current (19.4 μA) at which single-mode lasing becomes unstable are lower than those for the power pump profile. This difference is mainly caused by the fact that for the same axial current density, the total current of the beam for the power profile is 1.71 times higher than that for the hyper-Gaussian profile. Thus, the lasing threshold for the fundamental mode is achieved in both cases at approximately the same axial current density, but the critical excess of the lasing threshold for the next mode is somewhat higher for the power pump profile than for the hyper-Gaussian profile.

Because the line broadening factor R for structures studied in the experiment is poorly known, we performed a series of calculations for $R = 2.5$ and 5 for a fixed pump current $I_b = 35$ μA with the pump profile $f(\rho) = (1 + \rho^4)^{-1}$. Figure 6 shows the corresponding far-field intensity profiles for the generated mode. One can see that the output beam narrows down with increasing R and the far-field spot size broadens correspondingly. This demonstrates an important role of self-focusing caused by the gain saturation. The output power of the laser noticeably depends on the parameter R, being 2.41 and 1.2 mW for $R = 2.5$ and 5, respectively. The parameter M^2 was 1.17 for $R = 2.5$ and 1.06 for $R = 5$. Thus, the decrease in the output beam size is accompanied by some improvement of its quality, although the far-field divergence angle increases.

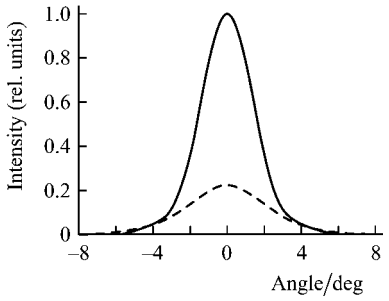

Figure 6. Far-field radiation intensity distribution for $R = 2.5$ (solid curve) and $R = 5$ (dashed curve); $I_b = 30$ μA; $f(\rho) = (1 + \rho^4)^{-1}$.

The divergence angle of the output beam was measured in experiments for a similar structure at beam currents noticeably exceeding the threshold value [15]. The typical value of the divergence angle was 15°. The beam divergence decreased approximately by a factor of 1.5 near the threshold. A theoretical model predicts the divergence angle of 11° for a small excess over the threshold. Taking into account the uncertainties in the value of R and the radial pump profile, the agreement with experiments is satisfactory.

4. Conclusions

The numerical method developed in the paper can be used to calculate the spatial profile, output power, wavelength, and other parameters of a generated mode in VCSELs. The characteristic calculation time of one resonance structure containing 25 QWs is about 1 h by using a Pentuim IV PC. By varying the pump current, it is possible to determine the lasing threshold, to study the single-mode lasing stability, and to find the maximum output power in this regime.

Acknowledgements. This work was partially supported by the Russian Foundation for Basic Research (Grant No. 08-02-00796-a).

References

1. Okhotnikov O.G. *Kvantovaya Elektron.*, **38**, 1083 (2008) [*Quantum Electron.*, **38**, 1083 (2008)].
2. Bogdankevich O.V., Goncharov V.A., Lavrushin B.M., Letokhov V.S., Suchkov A.F. *Fiz. Tekh. Poluprovodn.*, **1**, 7 (1967).
3. Bogdankevich O.V., Letokhov V.S., Suchkov A.F. *Fiz. Tekh. Poluprovodn.*, **3**, 665 (1969).
4. Bogdankevich O.V., Ulasyuk V.N. *Kvantovaya Elektron.*, **1**, 357 (1974) [*Sov. J. Quantum Electron.*, **4**, 198 (1974)].
5. Bogdankevich O.V., Goriev Yu.G., Darznek S.A., Katsap V.N., Tumanova L.A., Ulasyuk V.N. *Kvantovaya Elektron.*, **16**, 1775 (1989) [*Sov. J. Quantum Electron.*, **19**, 1141 (1989)].
6. Bogatov A.P., Eliseev P.G. *Kvantovaya Elektron.*, **12**, 465 (1985) [*Sov. J. Quantum Electron.*, **15**, 308 (1985)].
7. Bondarev V.Yu., Kozlovsky V.I., Krysa A.B., Popov Yu.M., Skasyrsky Ya.K. *Kvantovaya Elektron.*, **34**, 919 (2004) [*Quantum Electron.*, **34**, 919 (2004)].
8. Rao H., Steel M.J., Scarmozzino R., Osgood R.M. Jr. *IEEE J. Quantum Electron.*, **37**, 1435 (2001).
9. Elkin N.N., Napartovich A.P., Troshchieva V.N., Vysotsky D.V. *Lect. Notes Comp. Sci.*, **4310**, 542 (2007).
10. Fox A.G., Li T. *IEEE J. Quantum Electron.*, **QE-2**, 774 (1966).
11. Elkin N.N., Napartovich A.P., Troshchieva V.N., Vysotsky D.V. *Lect. Notes Comp. Sci.*, **5434**, 273 (2009).
12. Hadley G.R., Hohimer J.P., Owyoung A. *IEEE J. Quantum Electron.*, **23**, 765 (1987).
13. Siegman A.E. *Opt. Lett.*, **1**, 13 (1977).
14. Demmel J. *Applied Numerical Linear Algebra* (Philadelphia, PA: SIAM, 1997; Moscow: Mir, 2001).
15. Bondarev V.Yu., Kozlovsky V.I., Krysa A.B., Kuznetsov P.I., Sannikov D.A., Skasyrsky Ya.K., Tiberi M.D., Popov Yu.M. *Proc. SPIE Int. Soc. Opt. Eng.*, **6637**, 663707 (2007).